Biochemical Pharmacology 169 (2019) 113640

Contents lists available at ScienceDirect

Biochemical Pharmacology

journal homepage: www.elsevier.com/locate/biochempharm

FRET biosensor-based kinase inhibitor screen for ERK and AKT activity reveals differential kinase dependencies for proliferation in TNBC cells

Jichao He, Steven Wink, Hans de Bont, Sylvia Le Dévédec, Yinghui Zhang, Bob van de Water*

Division of Drug Discovery and Safety, Leiden Academic Centre for Drug Research, Leiden University, 2300 RA Leiden, the Netherlands

ARTICLE INFO

Keywords:
FRET
Kinase activity dynamics
TNBC
Drug resistance
Kinase dependencies

ABSTRACT

Enhanced expression and activity of protein kinases are critical in tumor cell proliferation and cancer progression. These various cancer-related kinases form intricate interdependent signaling networks. Evaluation of the effect of various kinase inhibitors on these networks is critical to understand kinase inhibitor efficacy in cancer therapy. The dynamic activation of some kinases can be monitored by fluorescence resonance energy transfer (FRET) biosensors with high temporal resolution. Here, we established a FRET biosensor-based high throughput imaging approach to determine ERK and AKT activity in two triple negative breast cancer (TNBC) cell lines HCC1806 and Hs578T. FRET functionality was systematically evaluated using EGF stimulation and different MEK and AKT inhibitors, respectively. Next, we assessed the effect of a kinase inhibitor library containing > 350 different kinase inhibitors (KIs) on ERK and AKT kinase activity using a FRET high-throughput screening setting. Suppression of FRET-ERK activity was generally positively correlated with the proliferation phenotype against inhibitors targeting MAPK signaling in both cell lines containing FRET-ERK reporter. AKT inhibitor (AKTi) resistant HCC1806 showed decreased proliferation associated with downregulated dynamics of FRET-ERK when treated with KIs targeting protein receptor tyrosine kinase (RTK). Yet, MEK inhibitor (MEKi) resistant Hs578T showed positively correlated FRET-AKT and proliferative responses against different PI3K and AKT inhibitors. Altogether, our data demonstrate the feasibility to integrate high throughput imaging-based screening of intracellular kinase activity using FRET-based biosensors in assessing kinase specificity and possible signaling crosstalk in direct relation to therapeutic outcome.

1. Introduction

Protein kinases constitute the complexity in signaling networks that orchestrate extracellular and intracellular signals to control cell growth, proliferation and survival [1–4]. Deregulation of kinase signaling cascades underlies the cause of cancer. Triple negative breast cancer (TNBC) is an aggressive subtype of breast cancer with unfavorable prognosis [5,6]. Advanced large-scale gene expression profiling has revealed several frequently altered signaling pathways in TNBC, including high expression of genes in epithelial-mesenchymal transition and growth factor pathways, enriched immune cell processes and androgen signaling, and increased cell cycle and DNA damage responses [7–9]. Particularly, overexpression of receptor tyrosine kinases (RTKs) and frequently elevated activation of MAPK/ERK and PI3K/AKT pathways, the two canonical pathways converging RTK signaling, have been observed in a set of TNBCs [10,11]. Therefore, kinase targeted therapies with diverse RTK inhibitors, MEK inhibitors (MEKi) and AKT inhibitors (AKTi) to block upregulated RTK, MAPK/ERK and PI3K/AKT signaling in TNBC have been explored under clinical investigation [12–14]. However, TNBC patients do not respond equally well to kinase targeted therapies, often encountering the problem of inhibitor resistance, due to upregulated adaptive signaling pathways or drug induced kinome reprogramming [15–19]. Hence, dissection of kinase dependency is essential for discovering effective kinase targeted therapeutics for the dismal TNBC.

Fluorescence resonance energy transfer (FRET) imaging has been explored in innovating the discovery of effective therapeutics for cancer therapy [20–23]. In particular, genetically encoded FRET biosensors that stably express two fluorescent proteins, mostly CFP and YFP (cyan and yellow fluorescent proteins), enable quantitative measurement of kinase dynamic activity and real-time monitoring of inhibitor-target potency in living cells [24]. FRET biosensors are developed based on phosphorylated peptide substrate of a kinase for its kinase activity [25] or based on

Abbreviations: FRET, fluorescence resonance energy transfer; TNBC, triple negative breast cancer; AKTi, AKT inhibitor; MEKi, MEK inhibitor; KI, kinase inhibitor; RTK, receptor tyrosine kinase; SRB, sulphorhodamine B; EGF, human epidermal growth factor; FACS, fluorescence activated cell sorting; CFP, cyan fluorescent protein; YFP, yellow fluorescent protein

* Corresponding author.
E-mail address: b.water@lacdr.leidenuniv.nl (B. van de Water).

https://doi.org/10.1016/j.bcp.2019.113640
Received 3 July 2019; Accepted 13 September 2019
Available online 16 September 2019

conformational changes of the kinase itself for its activation [26]. Substrate-based FRET biosensors have been extensively applied to evaluate the activities of kinase targets in response to kinase inhibitors. For example, a stably expressed FRET biosensor for epidermal growth factor receptor (EGFR) signaling in HeLa cells was reported to predict the efficiency of inhibitors targeting Ras-ERK and PI3K-S6K pathways [21]. A designed FRET kinase translocation reporter was described to dynamically measure multiple JNK, p38 and ERK activities in live single cells under inhibitor treatment [27]. A panel of optimized FRET biosensors have been established to monitor the kinase activities of PKA, ERK, JNK, EGFR/Abl, Rac1, RSK, S6K, AKT and PKC in response to EGF stimulation and kinase inhibitors [28,29]. Therefore, utilization of substrate-based FRET biosensor imaging may allow dissecting the complexity of kinase networks in drug-resistant TNBC cells and predicting effective kinase inhibitors for treating the refractory TNBC.

We have previously profiled the proliferative responses of 20 TNBC cell lines to 378 kinase inhibitors (Selleckchem®). Consistent to the clinical results, our results also demonstrated the differential response phenotype of TNBC cells to MEK and AKT targeted inhibitors, and defined the groups of MEKi-resistant and AKTi-resistant TNBC cell lines (van der Noord et al, Scientific Reports, 2019, in press). In this study, we described a FRET-ERK and FRET-AKT biosensor based high-throughput imaging approach to quantitatively monitor ERK and AKT dynamic activity in MEKi-resistant and AKTi-resistant TNBC cells in response to the 378 kinase inhibitors. We derived a mathematical model that associates MEK and AKT kinase activity with anti-proliferation effects, by which we revealed unique kinase dependencies on RTK/MAPK and PI3K/AKT pathways that are distinctly targetable in the resistant TNBC cells.

2. Materials and methods

2.1. Reagents and antibodies

A library of 378-kinase inhibitors (the L1200 library), BEZ235, AZD5363, erlotinib, gefitinib, selumetinib, GSK1059615, GSK690693 and TAK733 inhibitors were purchased from Selleckchem (Huissen, the Netherlands). The phospho(Ser473)-AKT (9271), phospho(Thr202/Tyr204)-p44/42 MAPK (ERK1/2, 9101), GFP (D5.1, 2956), AKT (9272) and p44/42 MAPK (ERK1/2, 4695) antibodies were from Cell Signaling (Bioké, Leiden, the Netherlands). The antibody against tubulin (T-9026), blasticidin S (15205) and human epidermal growth factor (EGF, E9644) were from Sigma Aldrich (Zwijndrecht, the Netherlands).

2.2. Cell culture

Human TNBC cell line HCC1806 and Hs578T were provided by Erasmus Medical Center (Rotterdam, the Netherlands). Cells were cultured in RPMI-1640 medium supplemented with 10% fetal bovine serum, 25 U/mL penicillin and 25 μg/mL streptomycin in a humidified incubator at 37 °C with 5% CO_2.

2.3. Establishment of stable FRET reporter cell line

Constructs of FRET biosensors for ERK (named pPBbsr-EKAREV-nls) and AKT (named pPBbsr-Eevee-iAKT-nes) have been described previously [28,29] and kindly provided by Prof. Dr. Michiyuki Matsuda (Laboratory of Bioimaging and Cell Signaling, Kyoto University, Japan). Stable cell lines expressing ERK-FRET and AKT-FRET biosensors using a transposon system were established, as described previously [22]. pCMV-mPBase (mammalian codon-optimized PBase) encoding a piggyBac transposase was a gift from Allan Bradley (Welcome Trust Sanger Institute, Cambridge, UK). HCC1806 and Hs578T cells were transfected with pCMV-mPBase and either pPBbsr-EKAREV-nls or pPBbsr-Eevee-iAKT-nes, and selected with blasticidin S at a dose of 2 μg/ml for 10 days to generate cells expressing EKAREV-nls or Eevee-iAKT. Plasmids were transfected using lipofectamine™ 3000 transfection reagent (Thermo Fisher Scientific, Waltham, USA) according to the manufacturer's instructions. Selected cells were suspended and further FACS (fluorescence activated cell sorting)-sorted at the Leiden University Medical Center flow cytometry core facility (Leiden, the Netherlands).

2.4. Cell proliferation assay

A sulforhodamine B (SRB) colorimetric assay was used to measure total amount of proteins indicative of cell proliferation [30]. Briefly, 4-day post-treatment, cells in 96-well plates were fixed with 30 μL 50% trichloroacetic acid for 1 h at 4 °C, followed by gently washing with tap water. Fixed and air-dried cells were stained with 60 μL of 0.4% SRB (dissolved in 1% acetic acid) at room temperature for 2 h. Unbound SRB was washed away with 1% acetic acid. The protein-bound SRB was solubilized in 10 mM unbuffered Tris base solution at room temperature for 2 h on a plate shaker and measured for its absorbance at 540 nm with an Infinite M1000 microplate reader (Tecan, Giessen, the Netherlands).

2.5. FRET KI library screen

Cells were seeded in 96-well plates at appropriate densities in complete medium and screened in duplicate against the 378-KI library (Selleckchem®) at 1 μM. Three basal images were captured prior to KI treatment. FRET imaging was automated continuously for 90 min in the presence of KIs, and proliferation assay was performed 4 days after treatment. All primary screening data results can be obtained from the corresponding author upon request.

2.6. siRNA transfection

To silence target genes, 50 nM siGENOME Human SMARTpool siRNA mix (GE Dharmacon, Lafayette, CO, USA) was transfected into cells by transfection reagent INTERFERin (Polyplus-Transfection SA, Illkirch-Graffenstaden, France) according to the manufacturer's instructions. The medium was refreshed 24 h post-transfection and transfected cells were used in experiments 48 h post-transfection.

2.7. Western blotting

Cells were seeded in 6-well plates at the appropriate density. For stimulation/starvation assays, medium was refreshed with serum-free medium (SFM) the following day and cells were starved overnight. Thereafter, cells were stimulated with 50 ng/ml EGF (Sigma; E9644) for 5 min in SFM. Cells were lysed with RIPA buffer containing 1% protease/phosphatase inhibitor cocktail (Sigma-Aldrich, P8340). Proteins were resolved by SDS-PAGE and transferred to polyvinylidine difluoride membranes. Membranes were blocked in 5% BSA in Tris-buffered saline with 0.05% Tween-20 (TBS-T), followed by overnight incubation with primary antibodies, washing, and 1 h incubation with HRP-conjugated secondary antibodies. Chemiluminescence was generated in the presence of HRP substrate and detected with an Amersham Imager 600 (GE Healthcare Life Sciences, Eindhoven, the Netherlands). Protein bands were quantified using ImageJ (NIH, US).

2.8. Time-Lapse imaging

Cells were imaged using a Nikon Eclipse Ti confocal microscope (Nikon, Amsterdam, The Netherlands) equipped with a PlanApoVC 20x/0.75 objective lens, a cooled CCD camera, a CoolLED pE-100 excitation light source, an automated stage and perfect focus system, and an incubation chamber. The dichroic mirrors and filters used for time-lapse imaging were as follows: a T640LPXR dichroic mirror, and emission filters FF01-482/35 and FF01-525/50 for CFP and FRET, respectively. All images were acquired using NIS software (Nikon). 408 nm LED lamp was used as light source, with 1.4% of lamp power. Acquisition times were 2 s for donor channel and 2 s for FRET at binning 2 × 2. Cells were plated in 96-well, collagen-coated,

glass-bottom plate (Greiner, Kremsmünster, Austria). After attachment, cells were imaged in phenol red-free RPMI-1640 medium at 37 °C. For EGF exposure study, cells were starved at least 12 h and treated with stimulus, followed by the addition of inhibitors if necessary. 3–5 frames were taken prior to any compound addition to obtain basal CFP and FRET intensity level.

2.9. FRET ratio image analysis

Image analysis was implemented using a combination of ilastik (v1.1.9) and CellProfiler (v2.1.1). Acquired images were split into the original channels. Segmentation was performed based on FRET images using ilastik. Mono-channel images were masked with segmentations using CellProfiler.

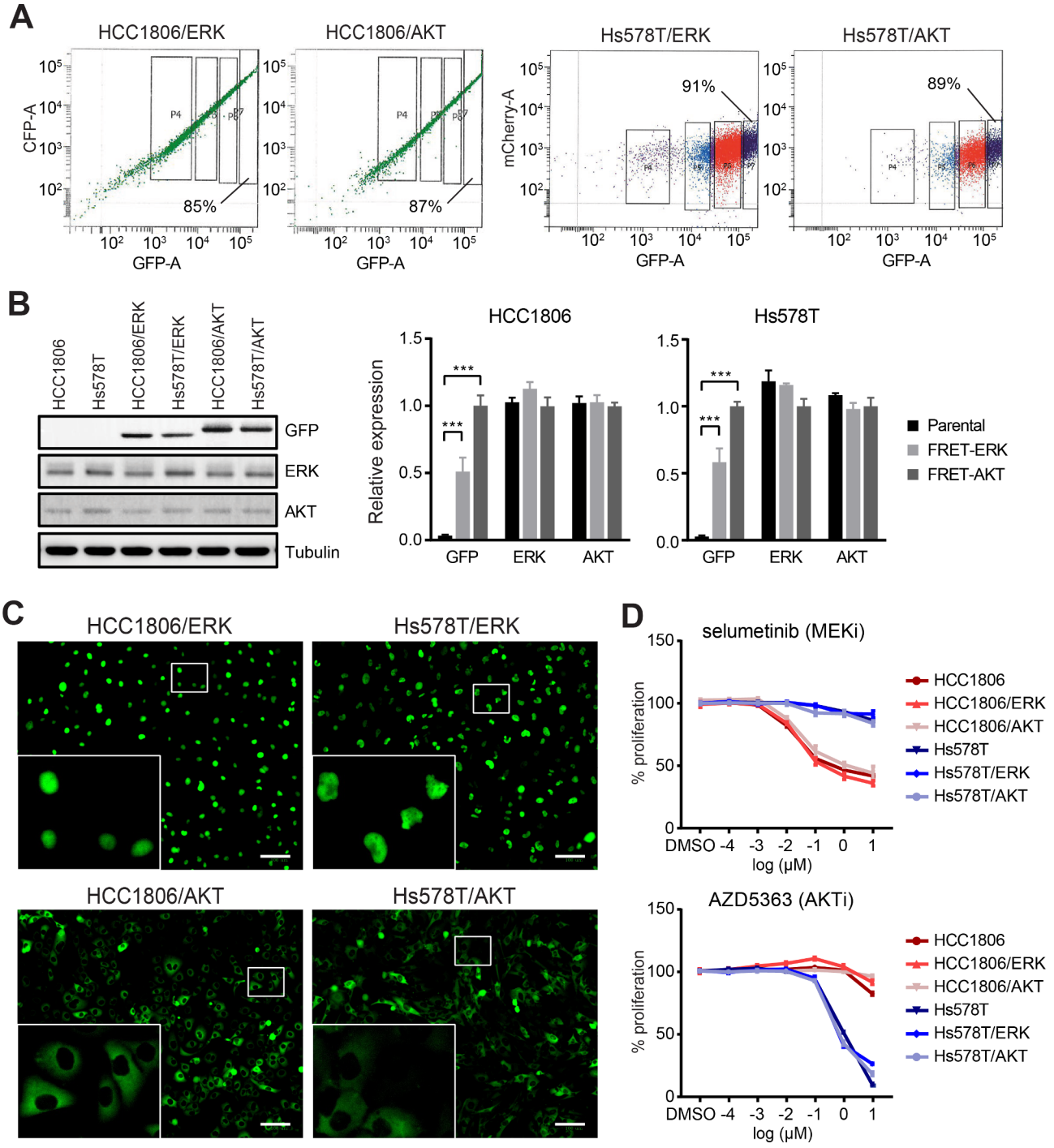

Fig. 1. Establishment of FRET reporter TNBC cell lines. (A) Percentage of FRET biosensor positive cells sorted by FACS. TNBC cells were transfected with DNA plasmids encoding FRET-ERK and -AKT biosensors and selected with blasticidin (20 μg/ml) for one week, followed by trypsinization and suspension prior to FACS. Cells from polyclones were used for FACS sorting. The percentage in each plot indicated the sorting efficiency. (B) Biosensor expression in FRET reporter cells. Antibody against GFP was used to detect fluorescence of expressed biosensors. Quantification of ERK, AKT and total fluorescent protein level in parental and FRET reporter TNBC cell lines. The expression level relative to Tubulin was normalized to that in each corresponding FRET-AKT cell line. (C) Fluorescence imaging of FRET reporter cells. Cells were imaged in GFP channel using ZOE™ fluorescent cell imager. Scale bar = 100 μm. (D) Effects of selumetinib and AZD5363 on cell proliferation of parental and FRET biosensors cell lines. Both parental and FRET-ERK (AKT) reporter HCC1806 and Hs578T cells were treated with selumetinib and AZD5363 in concentration range for 4 days, followed by SRB proliferation assay. The results were expressed as mean ± SEM of three independent experiments (two-way ANOVA * $p < 0.05$, ** $p < 0.01$, *** $p < 0.001$).

The FRET and CFP intensities were quantified per pixel and the FRET was divided by the CFP channel. In general, for all reporter cell lines and studies, for each frame, > 100 cells were captured for the intensity measurement. FRET/CFP ratio images were created to represent the FRET efficiency. In the intensity-modulated display mode, eight colors from red to blue are used to represent the FRET/CFP ratio. The FRET/CFP value prior to compounds exposure was averaged and used as the reference. The ratio of raw FRET/CFP value versus the reference value was defined as the normalized FRET/CFP value. FRET dynamics curve for each treatment was modeled using R (v3.2.2) and RStudio (v0.99.887) with an in-house developed "celloscillate" pipeline (Wink et al, manuscript in preparation). Extremes representing maximum FRET effect were extracted from fitted curves and defined as MaxMagnitudeFRET.

2.10. Statistical analysis

Pearson correlation analysis were performed using GraphPad Prism 7 with 95% confidence band. Significance was set at $r > 0.5$. All experiments were performed in at least three independent biological replicates. Data were expressed as mean ± SEM (standard error of mean). Statistical analysis was performed using two-way ANOVA (* $p < 0.05$, ** $p < 0.01$, *** $p < 0.001$) where necessary. The hierarchical clustering in heatmap was performed using CRAN pheatmap package in RStudio (v0.99.887).

3. Results

3.1. Establishment of stably expressed FRET-ERK and FRET-AKT biosensor in TNBC cells resistant to MEK or AKT inhibition

To monitor ERK and AKT dynamic activity in control of TNBC cell proliferation, we firstly ectopically expressed YPet/ECFP pair and substrate-based FRET-ERK biosensor (EKAREV) and FRET-AKT biosensor (EeveeiAkt) [28,29] into an AKTi-resistant TNBC cell line (HCC1806) and a MEKi-resistant TNBC cell line (Hs578T), respectively. Two stable FRET-ERK biosensor lines (HCC1806/ERK, Hs578/ERK) and two FRET-AKT biosensor lines (HCC1806/AKT, Hs578T/AKT) were established, overall achieving > 85% of fluorescent positive cell population (Fig. 1A) and high levels of FRET pair expression (GFP bands) (Fig. 1B, left panel). Ectopic expression of FRET-ERK and FRET-AKT biosensors did not affect the endogenous ERK and AKT levels, compared to parental cells (Fig. 1B). Moreover, the homogeneity of the fluorescent protein expression in the established FRET biosensors cells was visualized via GFP channel of fluorescent microscopy (Fig. 1C). In response to proliferative inhibition by MEKi selumetinib and AKTi AZD5363, HCC1806 FRET biosensor cells remained MEKi-sensitive and AKTi-resistant, while Hs578T FRET biosensor cells were AKTi-sensitive and MEKi-resistant, phenocopying the drug responses of parental cells (Fig. 1D).

3.2. FRET-ERK and FRET-AKT activity in the biosensor TNBC cells are responsive to EGF stimulation and MEK or AKT inhibition

Since ERK and AKT are essential effectors of EGF-triggered signaling cascades, we next evaluated FRET-ERK and FRET-AKT activity dynamics in the presence of EGF at 10, 25, 50 and 100 ng/ml concentrations, respectively. The ratio of fluorescence intensity of the YFP (acceptor) channel (FRET) versus fluorescence intensity of CFP (donor) channel (CFP), FRET/CFP, was used to represent the level of FRET-ERK and FRET-AKT kinase activities [15]. In Hs578T/ERK reporter cells, FRET-ERK activity was effectively induced by EGF even at low concentration of 10 ng/ml, peaking at 10 min post-exposure and declining gradually till 90 min (Fig. 2A; Supplementary videos 1 and 2). The rapid induction of FRET-ERK activity by EGF was also captured in HCC1806/ERK cells (Fig. 2B; Supplementary videos 3 and 4), but attenuated swiftly, compared to Hs578T/ERK cells. FRET-AKT activity in Hs578T/AKT reporter cells was immediately triggered upon EGF stimulation, being enhanced during the 90-min imaging period (Fig. 2C). The FRET-ERK and FRET-AKT activities did not show significant EGF dose dependency. The FRET/CFP detection window in our established FRET-ERK and FRET-AKT biosensor TNBC cells were consistent with that shown in the original publications [28,29]. It has been reported that FRET-ERK and AKT signal positively correlates with ERK and AKT phosphorylation [29,31–33]. Consistently, our western blot results confirmed the activation of p-ERK in Hs578T/ERK and HCC1806/ERK, and p-AKT in Hs578T/AKT biosensor cells, when stimulated with EGF in time course (5, 10, 30, 60 and 120 min, at 50 ng/ml) and in concentration range (10, 25, 50 and 100 ng/ml, for 5 min) (Fig. 2E–G, I–K). However, HCC1806/AKT cells did not show increased FRET-AKT activity in response to EGF exposure (Fig. 2D), although AKT phosphorylation was rapidly induced (Fig. 2H–L). Noteworthy, instant membrane ruffling in HCC1806/AKT cells (Supplementary videos 5 and 6), but not Hs578T cells (Supplementary videos 7 and 8), was observed upon the addition of EGF. As the FRET-AKT biosensors were expressed in cytoplasm, cellular shrinkage might affect the membrane growth factor receptor-mediated signal transduction and eventually the ratiometric FRET measurement [34–36].

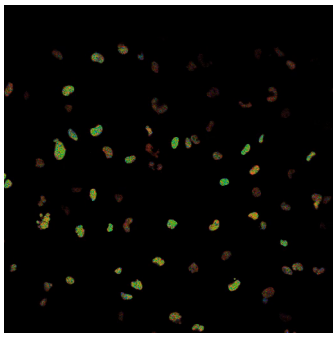

Supplementary video 1. Basal FRET-ERK activity dynamics in serum-starved Hs578T/ERK cells.

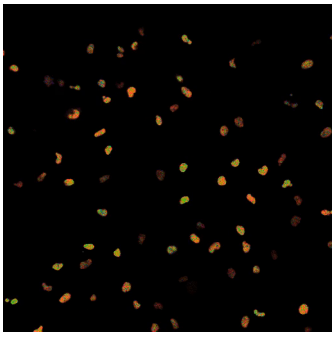

Supplementary video 2. EGF (50 ng/ml) stimulated FRET-ERK activity dynamics in serum-starved Hs578T/ERK cells.

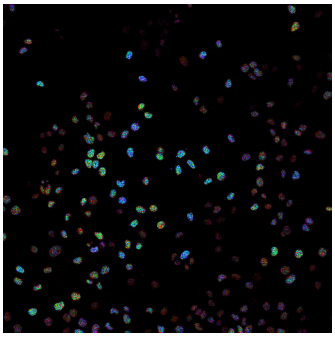

Supplementary video 3. Basal FRET-ERK activity dynamics in serum-starved HCC1806/ERK cells.

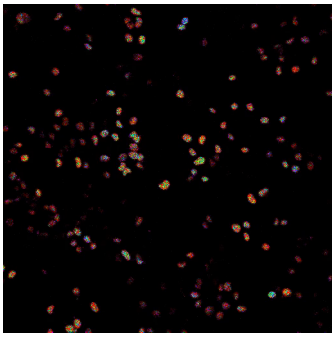

Supplementary video 4. EGF (50 ng/ml) stimulated FRET-ERK activity dynamics in serum-starved HCC1806/ERK cells.

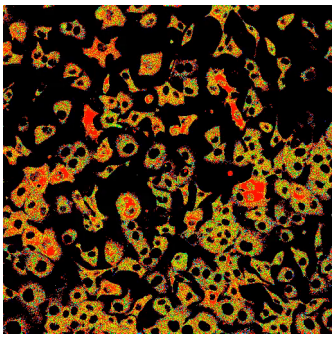

Supplementary video 5. Basal FRET-AKT activity dynamics in serum-starved HCC1806/AKT cells.

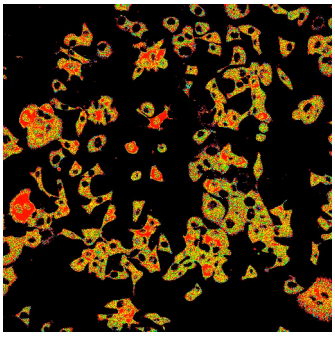

Supplementary video 6. EGF (50 ng/ml) stimulated FRET-AKT activity dynamics in serum-starved HCC1806/AKT cells.

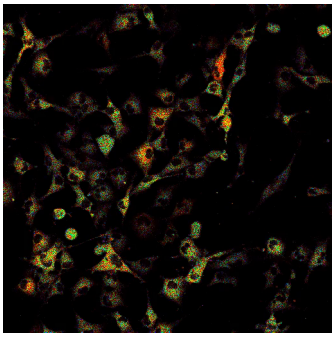

Supplementary video 7. Basal FRET-AKT activity dynamics in serum-starved Hs578T/AKT cells.

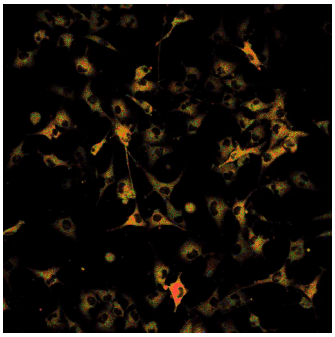

Supplementary video 8. EGF (50 ng/ml) stimulated FRET-AKT activity dynamics in serum-starved Hs578T/AKT cells.

Next, we demonstrated that the EGF-stimulated FRET-ERK activity in Hs578T/ERK cells was dropped down upon 20 min exposure to MEKi selumetinib in dose dependent manner (Fig. 3A), and the ratiometric FRET intensity was declined post 20 min of selumetinib exposure, as captured by time lapse imaging (Fig. 3B; Supplementary video 9). Similarly, the EGF-stimulated FRET-AKT activity in Hs578T/AKT cells was subject to the inhibitory effect of AKTi AZD5363 (Fig. 3C, D; Supplementary video 10).

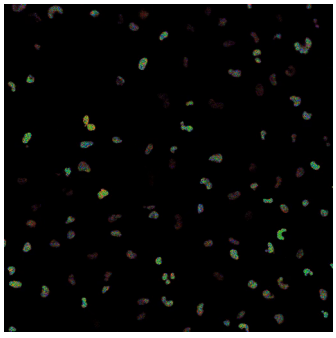

Supplementary video 9. Effects of MEKi selumetinib (1 μM) on FRET-ERK activity dynamics in the presence of EGF (50 ng/ml) in Hs578T/ERK cells.

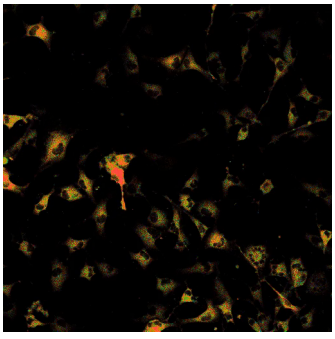

Supplementary video 10. Effects of AKTi AZD5363 (1 μM) on FRET-AKT activity dynamics in the presence of EGF (50 ng/ml) in Hs578T/AKT cells.

To clarify if the EGF-induced FRET kinase activity is attributed to EGFR signaling transduction upon EGF stimulation, we silenced EGFR and ERK2 in Hs578T/ERK cells by siRNA transfection, with AKT1 silencing as negative control. Knockdown of EGFR or ERK2, not AKT1, markedly blocked EGF-induced FRET-ERK activity in Hs578T/ERK cells

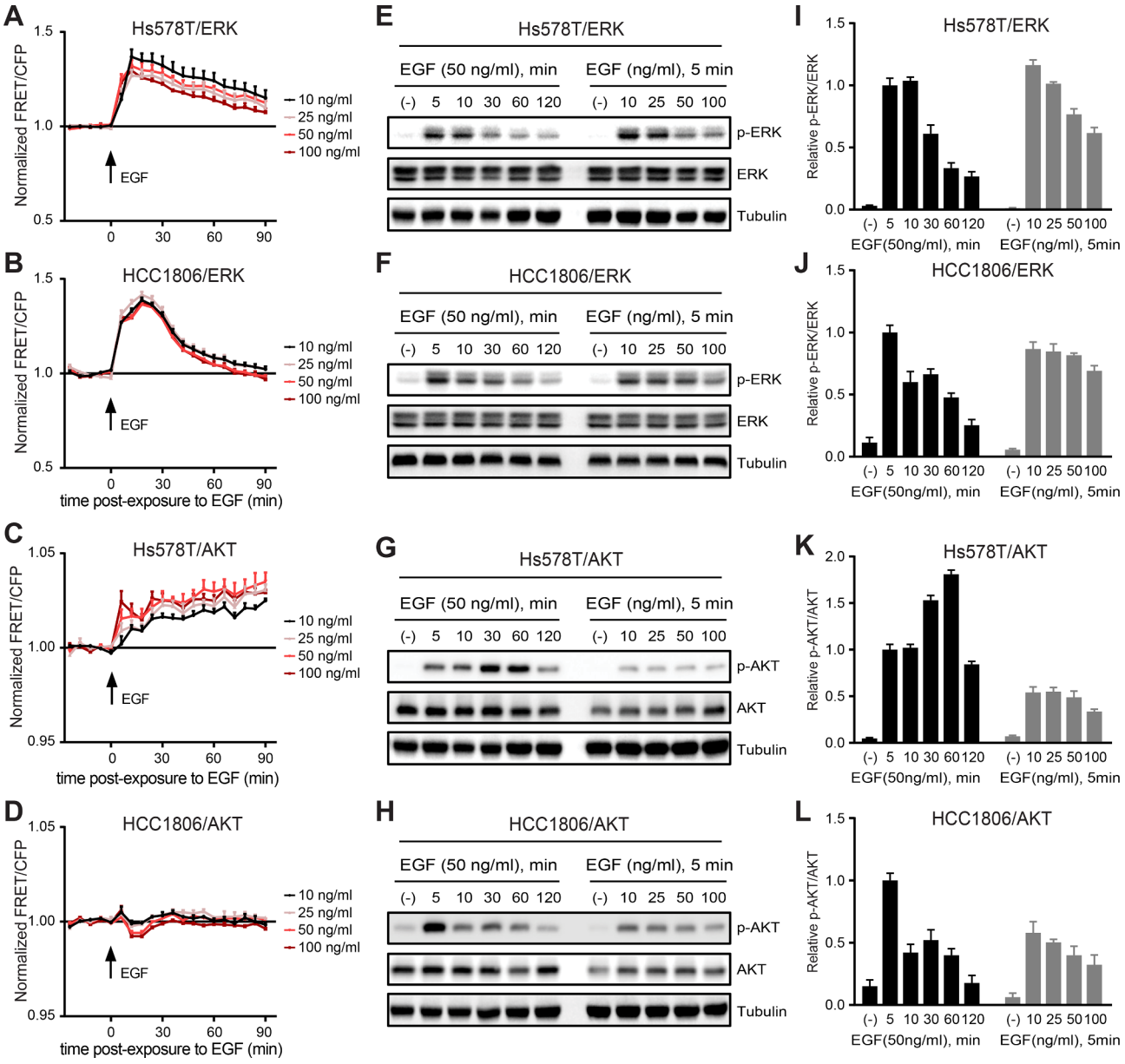

Fig. 2. FRET-ERK and FRET-AKT activity dynamics in response to EGF exposure. (A–D) Dynamics of FRET-ERK (A, B) and FRET-AKT (C, D) activity upon concentration range of EGF exposure. FRET reporter cells were serum-starved overnight and exposed to EGF at different concentrations. Five basal images were taken before EGF (ng/ml) was added. (E–H) Effects of EGF exposure on ERK (E, F) and AKT (G-H) phosphorylation. FRET reporter cells were serum-starved overnight and exposed to EGF in time course (left panel, 50 ng/ml) and concentration range (right panel, 5 min). (I–L) Quantification of phosphorylated ERK (I, J) and AKT (K, L) level, derived from (E–H). The expression level relative to total ERK or AKT was normalized to that in the sample exposed to EGF (50 ng/ml) for 5 min, the second bar. The results were expressed as mean ± SEM of three independent experiments.

(Fig. 4A) and moderately in HCC1806/ERK cells (Fig. 4B). The limited FRET-ERK blockade by silencing EGFR and ERK2 in HCC1806/ERK suggests that, besides EGFR and ERK2, other signaling components may contribute to the FRET-ERK activity in the AKTi-resistant cells.

Taking together, our established FRET-ERK and FRET-AKT biosensor TNBC cell models are applicable for capturing ERK and AKT dynamic activities in response to EGF/EGFR signaling cascades and inhibition of MAPK/ERK and PI3K/AKT upstream signaling pathways.

3.3. FRET-ERK and FRET-AKT imaging-based kinase inhibitor screening reveals multiple signaling pathways interacting with ERK and AKT kinase activity for TNBC cell proliferation

MAPK/ERK and PI3K/AKT pathways are the major intracellular mechanisms in response to extracellular signaling cues to control cell survival, proliferation, cell cycle and DNA damage [37–41]. To characterize ERK and AKT dynamic kinase activities in relation to kinase inhibition and proliferation in TNBC cells, we performed high-throughput FRET screening and proliferation screening with 378 inhibitors (Selleckchem®) targeting 118 kinases in the FRET-ERK and FRET-AKT biosensor TNBC cells above. FRET imaging was automated continuously for 90 min in the presence of kinase inhibitors (1 μM), and proliferation assay was performed 4 days after treatment. To evaluate FRET kinase activities in response to individual inhibitors, we modeled each temporal FRET dynamics curve based on FRET/CFP ratio and extracted fitted value for maximum FRET effect (MaxMagnitudeFRET). Pearson correlation analysis of the fitted value for each replicate showed high reproducibility of the FRET screening in each FRET biosensor cell line ($r > 0.8$, Fig. 5A–D). Pearson coefficient r for proliferation assays demonstrated high reproducibility of the replicate

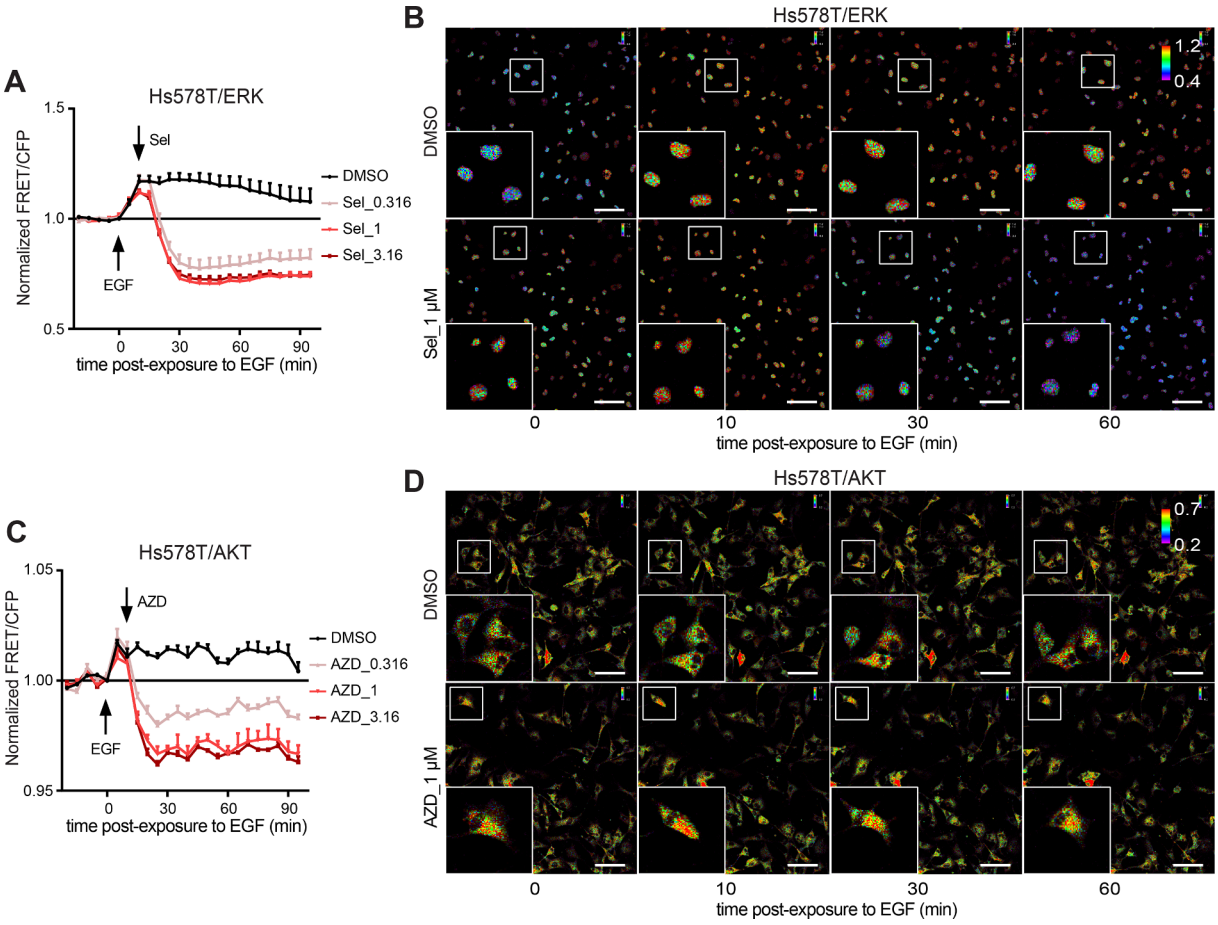

Fig. 3. Effects of MEK and AKT inhibitors on FRET-ERK and FRET-AKT activity. (A-D) Effects of selumetinib (Sel) and AZD5363 (AZD) on FRET-ERK (A-B) and FRET-AKT (C-D) activity dynamics in the presence of EGF. FRET reporter cells were serum-starved overnight and exposed to EGF at 50 ng/ml. Five basal images were taken before EGF was added. Arrow indicates when EGF, Sel or AZD was added; values represent μM. Raw FRET/CFP ratio was color-coded in rainbow scale. Scale bar = 100 μm. The results were expressed as mean ± SEM of three independent experiments.

proliferation screens ($r > 0.9$, Fig. 5E–H). The maximum FRET effect was plotted to relative proliferation for each kinase inhibitor for each FRET biosensor cell line. Given that the positive control for FRET-ERK (i.e. selumetinib) and FRET-AKT (i.e. AZD5363) achieved 0.8 and 0.96, respectively, we considered half maximum inhibitory effect on proliferation (50%) and FRET/CFP ratio 0.9 for FRET-ERK activity and 0.98 for FRET-AKT activity as effective inhibition. Consequently, 44 kinase inhibitors were screened to effectively inhibit both FRET-ERK activity and proliferation in HCC1806/ERK cells, while only 8 in Hs578T/ERK cells (Fig. 5I, J). In HCC1806/AKT and Hs578T/AKT biosensor cells, 14 and 26 inhibitors were selected, respectively (Fig. 5K, L). The FRET-ERK biosensor inhibitors mainly target signaling components in RTK and MAPK pathways, and the FRET-AKT effective inhibitors mostly suppress the kinases of PI3K/AKT pathway (Fig. 5M). The FRET-ERK and FRET-AKT biosensor inhibitors also block the signaling networks of angiogenesis, cell cycle, epigenetics, NF-κB, cytoskeletal signaling, JAK/STAT and DNA damage, indicating their interplay with MAPK/ERK and PI3K/AKT pathways.

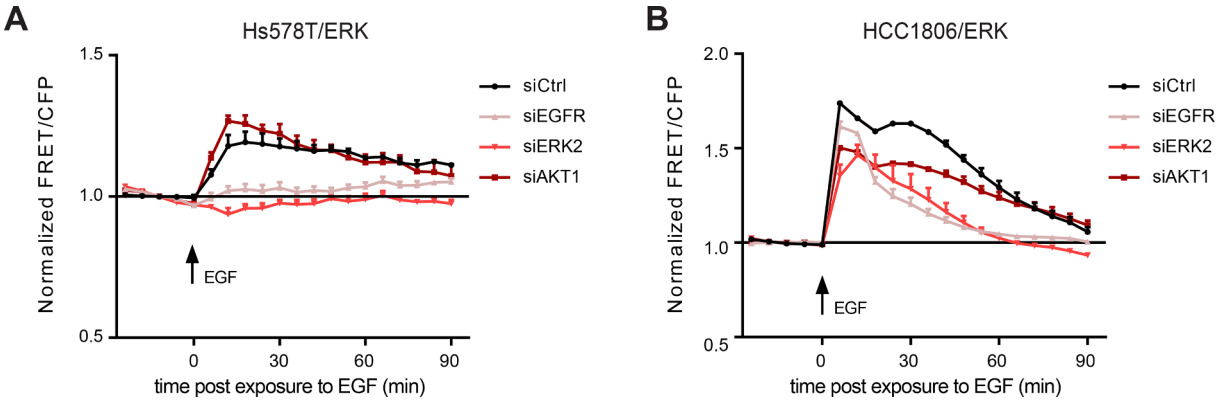

Fig. 4. EGFR and ERK played a role in EGF-stimulated FRET-ERK. (A, B) Effects of EGFR, ERK2 or AKT1 siRNA knockdown on EGF-stimulated FRET-ERK in Hs578T/ERK (A) and HCC1806/ERK (B) cells. FRET reporter cells were transfected with siRNAs for 48 h and serum-starved overnight prior to exposure to EGF at 50 ng/ml. Five basal images were taken before EGF was added. The results were expressed as mean ± SEM of three independent experiments.

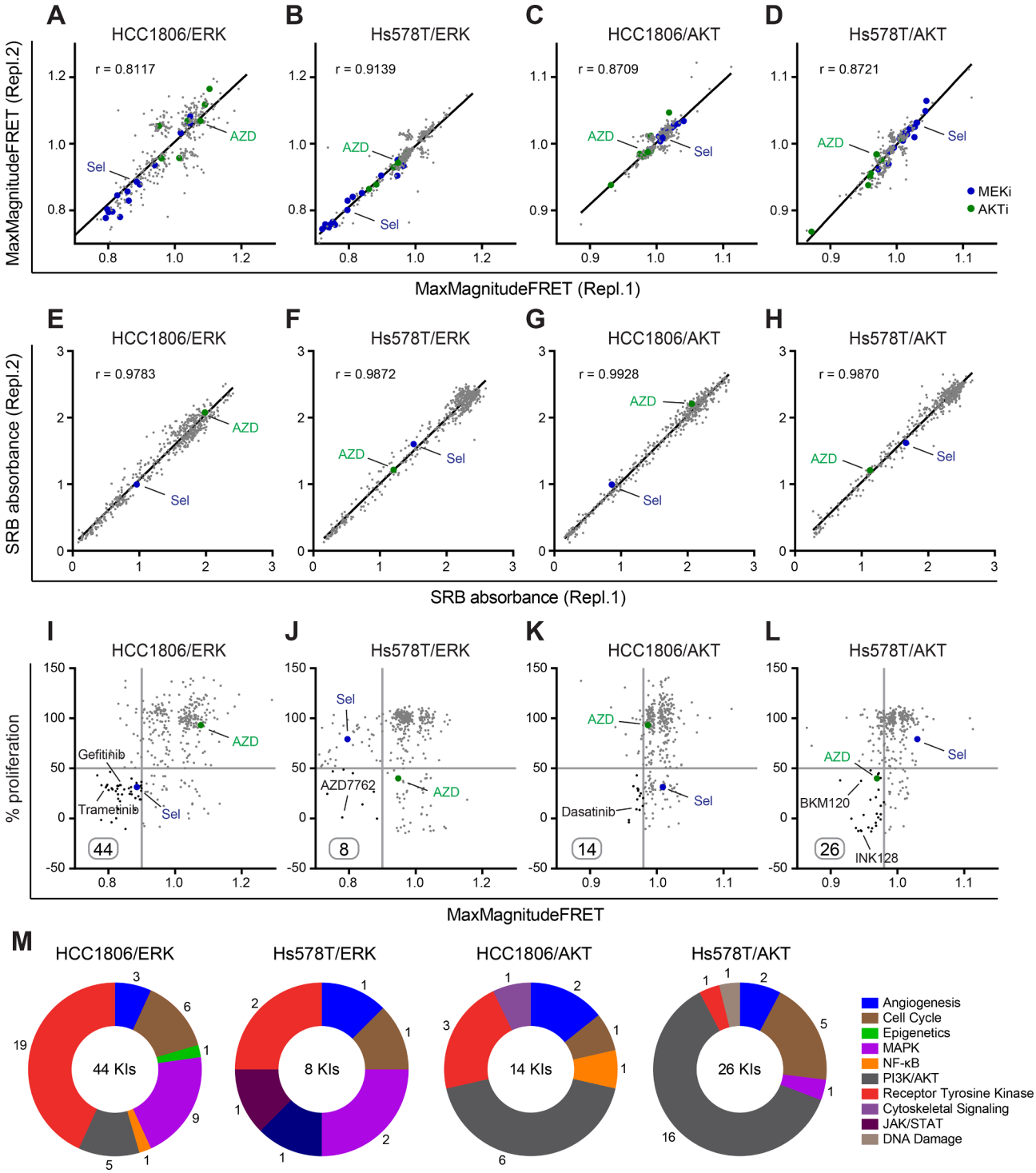

Fig. 5. FRET KI screen identifies differential kinase dependencies in TNBC cells. (A–H) Reproducibility of FRET kinase inhibitor (KI) screen on FRET (A–D) and cell proliferation (E–H). Pearson correlation coefficient r showing reproducibility of replicate screen in FRET reporter cells. Maximum magnitude FRET effect (MaxMagnitudeFRET) was extracted from fitted time-lapse FRET dynamic curve. Blue dots, MEKi. Green dots, AKTi. (I–L) Association of relative proliferation of each KI with maximum magnitude effects on FRET in reporter cell lines. KIs showing relative proliferation ≤ 50% and MaxMagnitudeFRET ERK (AKT) ≤ 0.9 (0.98) are numbered and circled. On the graphs displayed the averaged results of the replicate screen. (M) Donut plot of KIs selected from (I–L). Numbers of KIs and their targeted signaling pathways are annotated. (For interpretation of the references to color in this figure legend, the reader is referred to the web version of this article.)

3.4. FRET-ERK and FRET-AKT imaging for ERK and AKT activity visualizes RTK/MAPK and PI3K/AKT dependencies for TNBC cell proliferation

The observation above that RTK, MAPK and PI3K/AKT pathways were most frequently targeted by FRET-ERK and FRET-AKT biosensor inhibitors, suggests their essential role in TNBC cell proliferation. Next, we explored the relationship between the FRET effect (MaxMagnitudeFRET) and proliferation in response to inhibitors targeting RTK, MAPK and PI3K/AKT pathways. In response to MAPK inhibitors (MAPKi), both HCC1806 and Hs578T FRET-ERK biosensor cell lines displayed strong positive correlation between cell proliferation

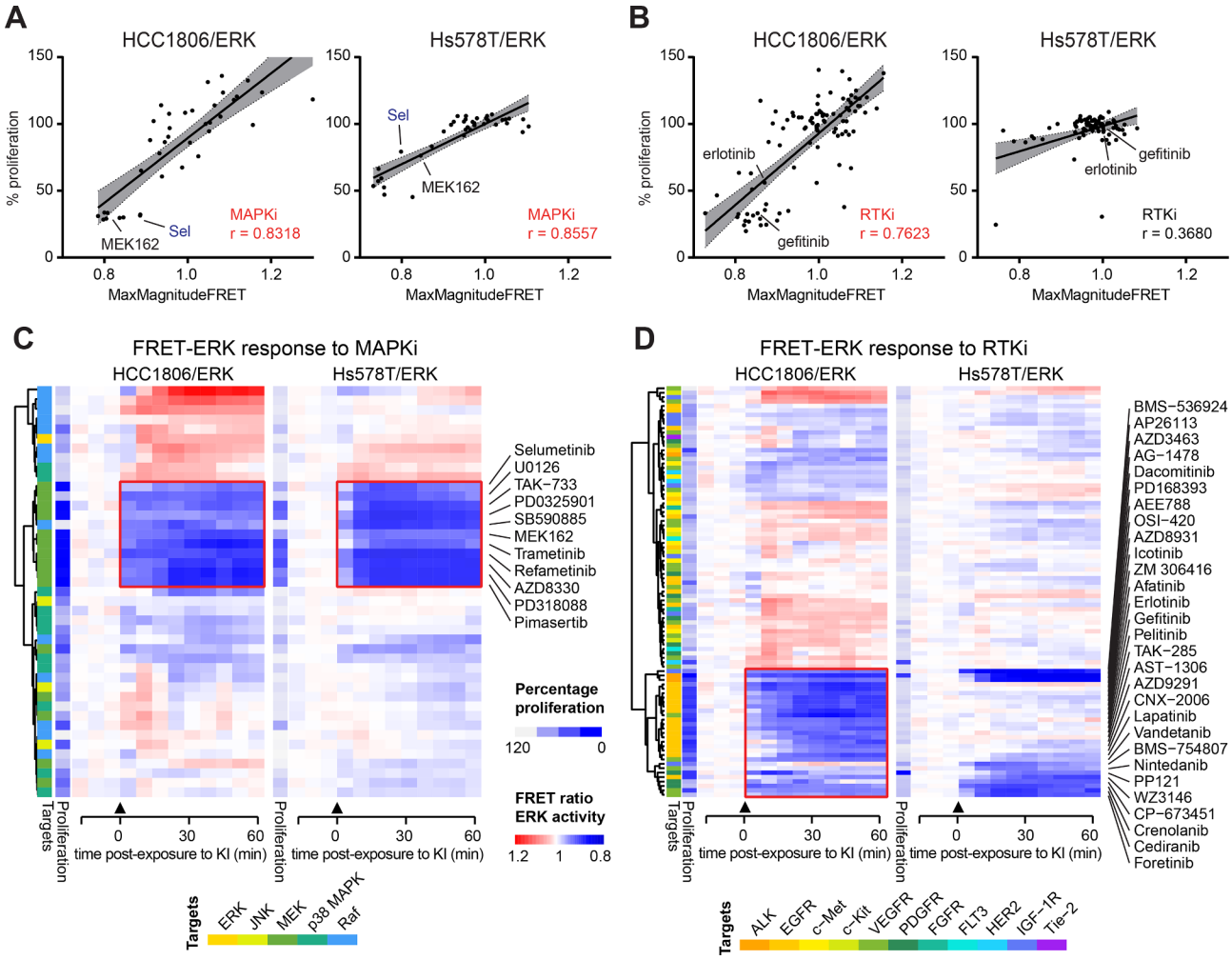

Fig. 6. Correlation between inhibition of FRET-ERK and cell proliferation by selective kinase inhibitors. (A, B) Association of MaxMagnitudeFRET with relative proliferation of KIs targeting MAPK signaling (MAPKi, A) and Receptor tyrosine kinase (RTKi, B) in FRET-ERK reporter cells. 95% confidence band is shown in grey. Significance is set at Pearson correlation coefficient r > 0.5 (red). (C, D) Clustering of FRET-ERK activity dynamics against MAPKi (C) and RTKi (D). Heatmaps were vertically clustered across KIs, annotated with relative proliferation and corresponding targets. FRET/CFP ratio was normalized to DMSO control. Arrow indicates when KIs were added. (For interpretation of the references to color in this figure legend, the reader is referred to the web version of this article.)

and FRET-ERK activity (r = 0.8318 and r = 0.8557, respectively) (Fig. 6A). While the proliferation of HCC1806/ERK cells was highly related to RTK-mediated FRET-ERK activity (r = 0. 7623), Hs578T/ERK cells were poorly responsive to RTK inhibitors (RTKi) with low correlation (r = 0.3680) in proliferation and FRET-ERK activity (Fig. 6B). Furthermore, hierarchical analysis of time-resolved FRET dynamics data clustered the MAPKi effect on FRET-ERK biosensor cells, revealing some MEK inhibitors correlatively inhibiting FRET-ERK activity and proliferation in both HCC1806/ERK and Hs578T/ERK cells (Fig. 6C). A group of RTKi, including EGFR inhibitors (EGFRi), displayed concurrent inhibitory effect on FRET-ERK activity and proliferation in HCC1806/ERK cells, not in Hs578T/ERK cells (Fig. 6D), indicating the RTKi resistance in Hs578T cells.

In FRET-AKT biosensor cells, positive correlation in FRET-AKT activity and proliferation was monitored in Hs578T/AKT cells when treated with PI3K inhibitors (PI3Ki, r = 0.7383) or AKT inhibitors (AKTi, r = 0.5534), whereas HCC1806/AKT cells were less responsive to PI3K/AKT inhibition (Fig. 7A, B). Consistently, FRET-AKT dynamics clustering displayed the sensitivity to PI3K/AKT signaling inhibition in Hs578T/AKT cells, but resistance in HCC1806/AKT cells (Fig. 7C, D).

Altogether, our integrated FRET biosensor and kinase inhibitor screening dissects the RTK/MAPK-dependent proliferation in HCC1806 TNBC cells that are resistant to PI3K/AKT inhibition, and the PI3K/AKT-dependent proliferation in Hs578T TNBC cells that are RTKi/MEKi-resistant.

3.5. MEKi-resistant and AKTi-resistant TNBC cells display differential FRET-ERK and FRET-AKT dynamics in response to RTK/MAPK and PI3K/AKT inhibition

To confirm the findings on kinase signaling dependencies in AKTi-resistant HCC1806 and RTKi/MEKi-resistant Hs578T TNBC cells, we further investigated the inhibitory effects of RTK/MAPK and PI3K/AKT inhibitors in escalating doses (0.316, 1 and 3.16 μM) on FRET-ERK and FRET-AKT dynamics in the FRET-ERK and FRET-AKT biosensor cell lines. Treatment with MEKi, selumetinib decreased FRET/CFP ratio in HCC1806/ERK and more significantly in Hs578T/ERK cell lines in a dose dependent fashion, while TAK733 effectively inhibited FRET-ERK activity even at low dose (0.316 μM) in both cell lines (Fig. 8A, upper panels). Distinctively, EGFRi gefitinib and erlotinib dramatically decreased FRET-ERK signal in HCC1806/ERK cells, but hardly ever in Hs578T/ERK cells (Fig. 8A, lower panels), revealing the EGFRi resistance in Hs578T cells. These differential FRET-ERK dynamic changes in HCC1806/ERK and Hs578T/ERK cells were captured, representatively upon 30 min exposure to MEKi selumetinib and TAK733 and EGFRi geftinib and erlotinib at 1 μM (Fig. 8B).

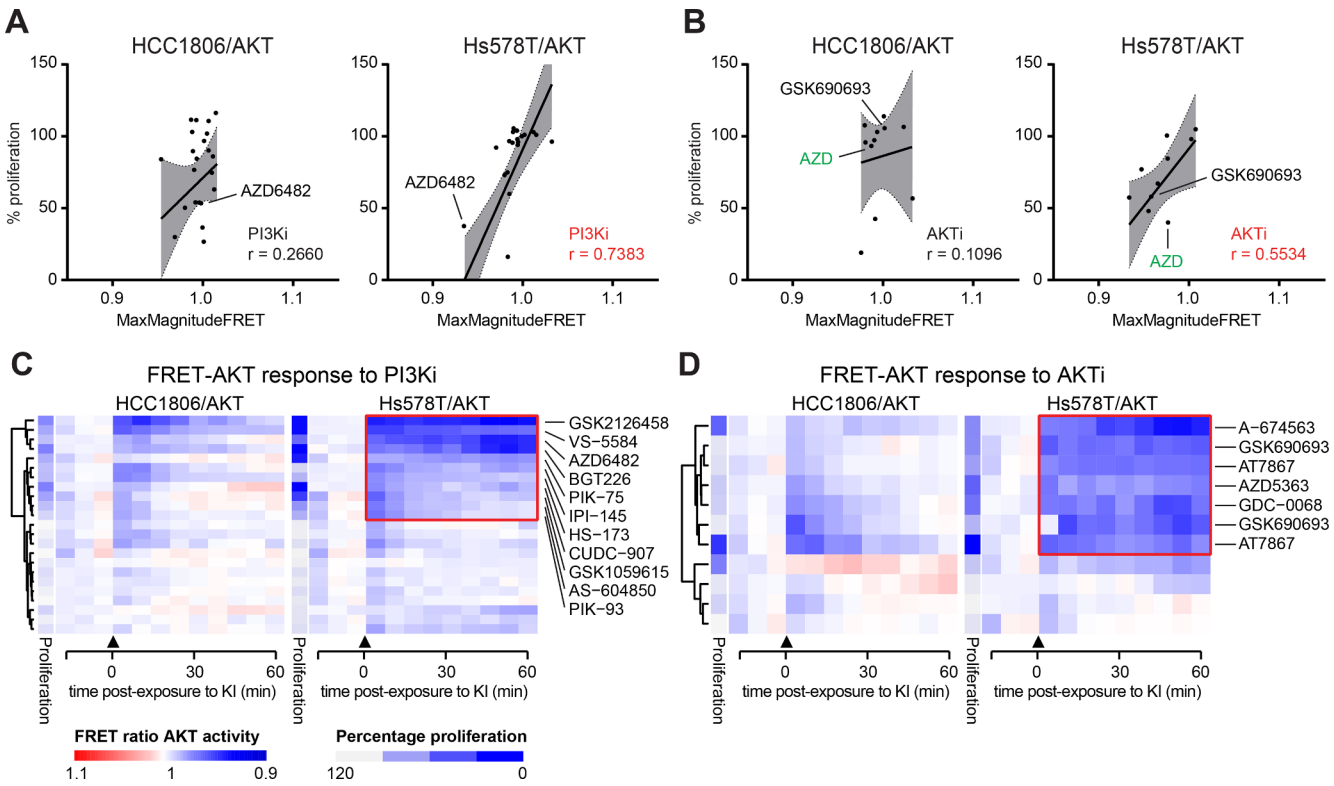

Fig. 7. Correlation between inhibition of FRET-AKT and cell proliferation by selective kinase inhibitors. (A, B) Association of MaxMagnitudeFRET with relative proliferation of KIs targeting PI3K (PI3Ki, A) and AKT (ATKi, B) in FRET-AKT reporter cells. 95% confidence band is shown in grey. Significance is set at Pearson correlation coefficient r > 0.5 (red). (C, D) Clustering of FRET-AKT activity dynamics against PI3Ki (C) and AKTi (D). Heatmaps were vertically clustered across KIs, annotated with relative proliferation and corresponding targets. FRET/CFP ratio was normalized to DMSO control. Arrow indicates when KIs were added. (For interpretation of the references to color in this figure legend, the reader is referred to the web version of this article.)

Next, PI3Ki and AKTi conferred inhibitory effect on FRET-AKT activity in both HCC1806/ERK and Hs578T/AKT cell lines, yet, in different patterns. The inhibited FRET-AKT by PI3Ki GSK1059615 and BEZ235 in HCC1806/ERK cells was gradually recovered within one hour, whilst the FRET-AKT in Hs578T cells was steadily restrained in dose dependence (Fig. 8C, left panels). AKTi AZD5363 and GSK690693 suppressed FRET-AKT activity more effectively in Hs578T/AKT cells than in HCC1806/AKT cells (Fig. 8C, right panels).

As a result, our FRET biosensor-based live imaging deciphered the ERK dynamic responsiveness to EGFRi in AKTi-resistant HCC1806 TNBC cells and the AKT dynamic responsiveness to PI3Ki and AKTi in MEKi-resistant Hs578T cells that are also highly refractory to EGFRi.

3.6. *EGFRi-refractory TNBC cells sustain ERK signaling for proliferation*

In EGFRi-refractory Hs578T TNBC cells, EGFRi failed to inhibit FRET-ERK activity, while the FRET-AKT activity was targetable by PI3Ki and AKTi, suggesting that the downstream ERK signaling bypasses EGFR inhibition, leading to resistance. Thus, we further addressed how the FRET-ERK dynamic activity is associated with proliferative responses to EGFRi, MEKi, PI3Ki and AKTi, respectively, in dose ranges. The proliferation assays demonstrated that Hs578T/ERK cells were highly resistant to EGFRi (gefitinib and erlotinib), maintaining low sensitivity to MEKi (selumetinib and TAK733) and highly responding to PI3Ki (BEZ235) and AKTi (AZD5363) (Fig. 9A, left). Contrastingly, the AKTi-resistant HCC1806/ERK cells were responsive to EGFRi and MEKi but relatively insensitive to PI3Ki and AKTi (Fig. 9A, right). Next, we assessed if the FRET-ERK activity dynamics would reflect the ERK phosphorylation status in Hs578T/ERK and HCC1806/ERK cells in response to representative inhibitors. Strikingly, EGFRi gefitinib eliminated ERK phosphorylation (p-ERK) in HCC1806/ERK cells, but left the downstream p-ERK signaling intact in Hs578T/ERK cells (Fig. 9B, C). MEKi suppressed ERK phosphorylation in both cell lines, correlating with downregulated FRET-ERK activity dynamics, while PI3Ki and AKTi conferred no significant changes on p-ERK status in the cells, as expected. Taken together, the FRET-ERK dynamic activity was indicative of ERK signaling and proliferation of TNBC cells in response to inhibition of signaling pathways, such as RTK, MAPK and PI3K/AKT.

4. Discussion

TNBC is an aggressive disease with unfavorable prognosis [5,6]. Currently, there are no effective targeted therapies approved for the treatment of TNBC patients. Given the pivotal role of EGFR/MAPK and PI3K/AKT signaling in controlling cell growth, survival and proliferation, central nodes of these pathways, MEK and AKT, have been emerging as promising targets for cancer drug discovery [42,43]. MEK inhibitors and AKT inhibitors have been explored for the treatment of TNBC in the past decades. However, the clinical outcomes are unfavorable due to drug-induced activation of alternative survival signaling pathways [15,44]. Here we have established and systematically characterized a panel of FRET-ERK and FRET-AKT TNBC reporter cell lines. We have applied this FRET reporter panel in high-throughput screening to uncover contextual kinase signaling dependencies in TNBC that modulate AKT and ERK pathways. Thus, we identified ten signaling pathways associated with the proliferative response of TNBC to kinase drugs.

Different TNBC cell lines demonstrate alternative resistance to AKT or MEK inhibitors, suggesting dependencies on either ERK or AKT signaling for their enhanced proliferation. In AKTi-resistant cells, targeting various receptor tyrosine kinases, MAPKs, cell cycle-related kinases, PI3K/AKT and angiogenesis caused a downregulation of FRET-ERK

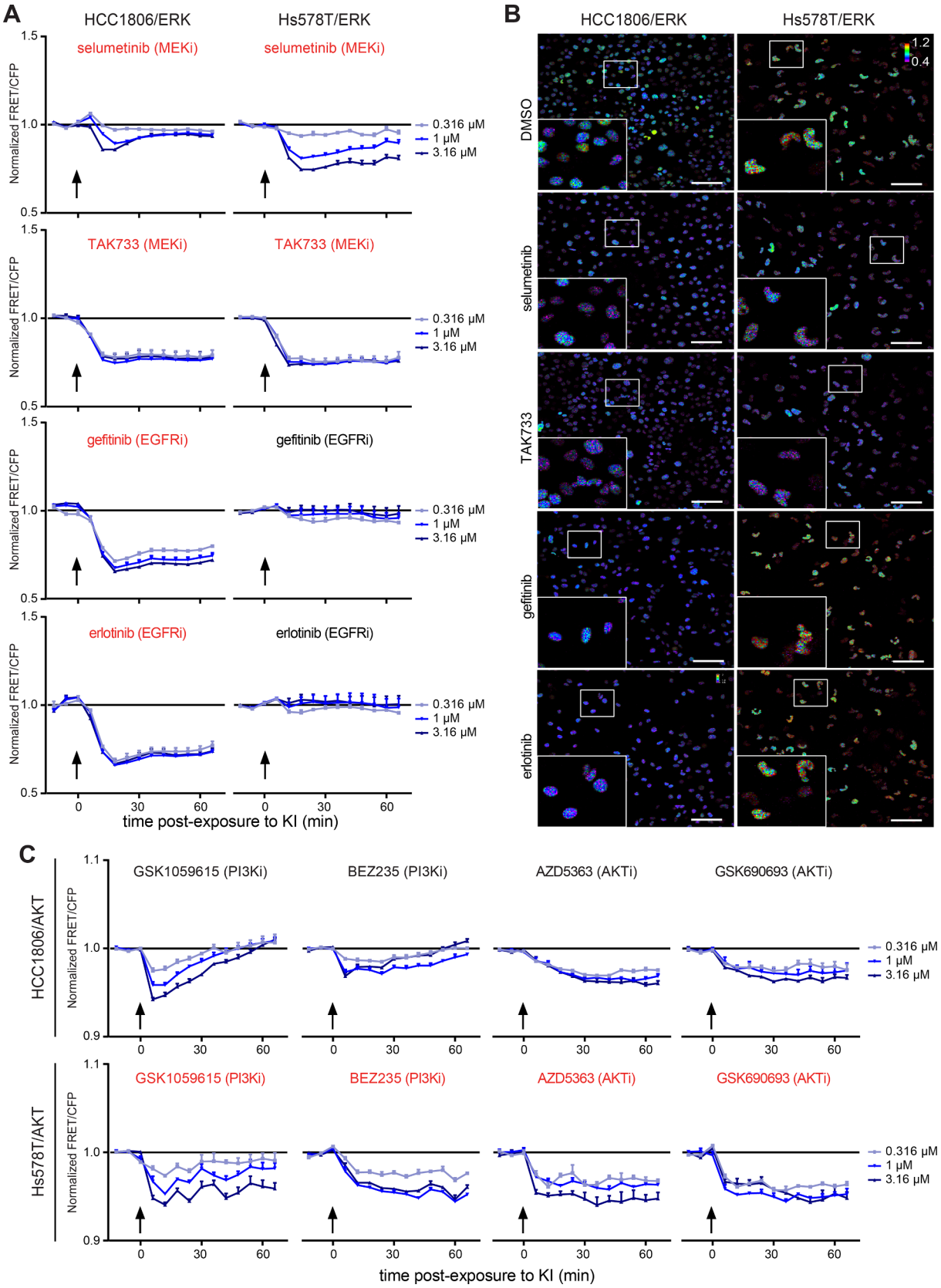

Fig. 8. Potency of selected kinase inhibitors on FRET-ERK and FRET-AKT activity. (A) Concentration response FRET-ERK activity dynamics for selumetinib, TAK733, gefitinib and erlotinib. (B) Representative images taken from (A) at 1 μM. Raw FRET/CFP ratio was color-coded in rainbow scale. Scale bar = 100 μm. (C) Concentration response of FRET-AKT activity dynamics for GSK1059615, BEZ235, AZD5363 and GSK690693. Three basal images were taken prior to KI treatment in dose range (μM). KIs showing positive correlation between MaxMagnitudeFRET and proliferation are marked in red. Arrow indicates when KIs were added. The results were expressed as mean ± SEM of three independent experiments. (For interpretation of the references to color in this figure legend, the reader is referred to the web version of this article.)

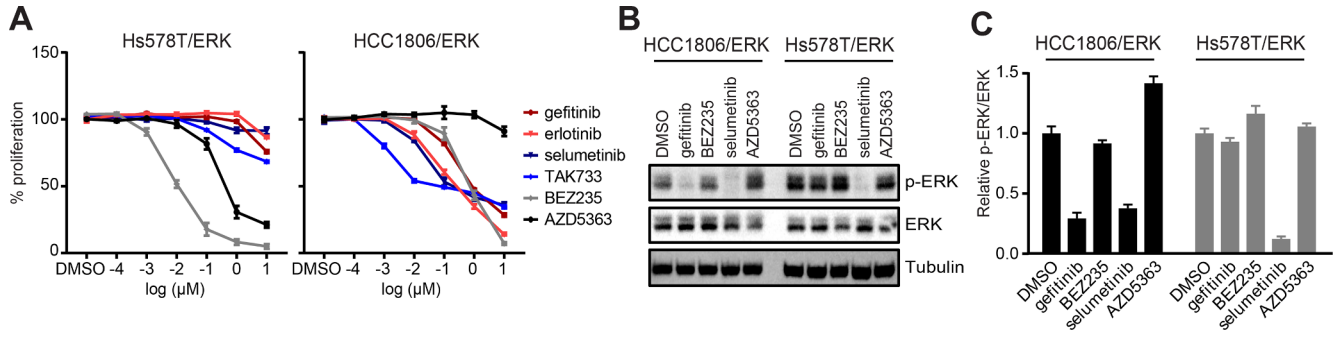

Fig. 9. Differential response of TNBC cells to inhibitors targeting different kinase signaling components. (A) Proliferative response of FRET-ERK reporter cells to EGFRi (gefitinib and erlotinib), MEKi (selumetinib and TAK733), PI3Ki BEZ235 and AKTi AZD5363 in a concentration range. (B) Effects of representative KI gefitinib, BEZ235, selumetinib and AZD5363 on ERK (AKT) phosphorylation in FRET-ERK (AKT) reporter cells. FRET reporter cells were treated with KIs at 1 μM for 30 min. (C) Quantification of phosphorylated ERK level, derived from (B). The expression level was normalized to total ERK and further compared to that in DMSO-treated cells. The results were expressed as mean ± SEM of three independent experiments.

dynamics, accompanied by attenuated proliferation. This included inhibitors targeting VEGFR (ZM 306,416 and AEE788), ALK (AP26113), MEK (TAK733), cell cycle (AZD7762 and TAK901), and Src (dasatinib). MEKi-resistant cells were addicted to PI3K/AKT and cell cycle regulated FRET-AKT activity. Further, we note that targeting PI3K/AKT and angiogenesis pathways did suppress FRET-ERK activity.

The MAPK signaling and PI3K/AKT signaling are two canonical pathways of RTK signal transduction, functioning in a variety of cellular processes [1,45]. Transcriptomics and proteomics profiles on TNBC samples indicate that activation of both pathways is frequently observed, but can be attributed to variable reasons. Ras and Raf are rarely mutated in TNBC [7,9]. However, activation of upstream RTKs and inactivation of negative regulators, such as NF1 mutation and DUSP4 loss, lead to active MAPK signaling [15,46–48]. Activation of PI3K pathway, either directly by PI3KCA mutation or indirectly by PTEN or INPP4B loss, is common in TNBC tumors [7,9,49]. Our KI screening data have demonstrated that the effects of MAPK inhibition on TNBC cell proliferation positively correlate with their efficacy on ERK activity. The inhibitory effects of RTKi on cell proliferation and ERK activity are better correlated in RTKi/MEKi-resistant cells than AKTi-resistant cells. Inhibition of PI3K/AKT signaling is efficacious to suppress cell proliferation in RTKi/MEKi-resistant subgroups. Complementary to accumulating molecule signature studies, our findings on differential kinase dependencies using our FRET reporter panel, provide experimental evidence for the development and prioritization of precision medicine for TNBC cohorts.

Kinase drugs have been preferably pursued as promising targeted therapeutics due to the pivotal role of kinase molecules in signal transductions and corresponding cell biological processes [14,43,50]. Given the hypothesis that kinases with enhanced expression or activating mutations hold the essentialities in cancer cell progression, gene expression signatures have been extensively studied and employed to identify common genetic background within cancer types [51,52]. However, a number of studies suggest that gene expression is rarely indicative of kinase activity, perturbation of which is a key factor for evaluating the effectiveness of kinase drugs [53,54]. In this study, establishment of high-content FRET-based live cell imaging enables dynamic quantitative detection of intracellular activity of ERK and AKT, two key elements in kinase signaling cascades. Our results illustrate that the influences on kinase activity incarnate the proliferative response of TNBC to kinase drugs in a temporal and direct way. We anticipate that FRET-based signaling reporters will contribute substantially to monitor the efficacy of candidate kinase inhibitors, but also will contribute to the further understanding of their mode-of-action in relation to crosstalk with well-defined signaling components in cancer, including ERK and AKT signaling.

In summary, our work describes an integrated protein kinase dependency identification and functional validation approach that identifies TNBC kinase addictions, potential targetable pathways and associated targeted therapeutics. We demonstrate the feasibility of FRET imaging-based high-content screening of intracellular kinase activity in assessing kinase specificity and possible signaling crosstalk. In particular, our study reveals the intact ERK kinase signaling which drives TNBC drug resistance against RTKi/MAPKi-targeted therapies. Besides RTKi and MAPKi, AKTi-resistant cells are also responsive to cell cycle inhibition via ERK downregulation. Future studies should aim at broadening the range of cancer relevant kinase biosensors and translating this approach to in vitro/in vivo models that are closer to the clinic, including cultures of patient-derived xenograft.

Declaration of Competing Interest

The authors declare that they have no known competing financial interests or personal relationships that could have appeared to influence the work reported in this paper.

Acknowledgments

This work was supported by the ERC Advanced grant Triple-BC (grant no. 322737). JH was financially supported by the China Scholarship Council.

Author contributions

JH, YZ and BvdW conceived and designed the experiments. YZ and BvdW supervised the research. JH and YZ performed the experiments. SW performed high-throughput imaging analyses. HdB and SLD helped with microscopy imaging and image segmentation. JH, YZ and BvdW wrote the manuscript. All authors read, reviewed and approved the final manuscript.

References

[1] M.A. Lemmon, J. Schlessinger, Cell signaling by receptor tyrosine kinases, Cell 141 (7) (2010) 1117–1134.
[2] J.S. Logue, D.K. Morrison, Complexity in the signaling network: insights from the use of targeted inhibitors in cancer therapy, Genes Dev. 26 (7) (2012) 641–650.
[3] Y. Yarden, M.X. Sliwkowski, Untangling the ErbB signalling network, Nat. Rev. Mol. Cell Biol. 2 (2) (2001) 127–137.
[4] E.D. Fleuren, L. Zhang, J. Wu, R.J. Daly, The kinome 'at large' in cancer, Nat. Rev. Cancer 16 (2) (2016) 83–98.
[5] R.L. Siegel, K.D. Miller, A. Jemal, Cancer statistics, 2018, CA Cancer J. Clin. 68 (1) (2018) 7–30.
[6] R. Dent, M. Trudeau, K.I. Pritchard, W.M. Hanna, H.K. Kahn, C.A. Sawka, L.A. Lickley, E. Rawlinson, P. Sun, S.A. Narod, Triple-negative breast cancer: Clinical features and patterns of recurrence, Clin. Cancer Res. 13 (15) (2007) 4429–4434.
[7] N. Cancer Genome Atlas, Comprehensive molecular portraits of human breast tumours, Nature 490 (7418) (2012) 61–70.
[8] B.D. Lehmann, J.A. Bauer, X. Chen, M.E. Sanders, A.B. Chakravarthy, Y. Shyr,

J.A. Pietenpol, Identification of human triple-negative breast cancer subtypes and preclinical models for selection of targeted therapies, J. Clin. Invest. 121 (7) (2011) 2750–2767.
[9] S.P. Shah, A. Roth, R. Goya, A. Oloumi, G. Ha, Y. Zhao, G. Turashvili, J. Ding, K. Tse, G. Haffari, A. Bashashati, L.M. Prentice, J. Khattra, A. Burleigh, D. Yap, V. Bernard, A. McPherson, K. Shumansky, A. Crisan, R. Giuliany, A. Heravi-Moussavi, J. Rosner, D. Lai, I. Birol, R. Varhol, A. Tam, N. Dhalla, T. Zeng, K. Ma, S.K. Chan, M. Griffith, A. Moradian, S.W. Cheng, G.B. Morin, P. Watson, K. Gelmon, S. Chia, S.F. Chin, C. Curtis, O.M. Rueda, P.D. Pharoah, S. Damaraju, J. Mackey, K. Hoon, T. Harkins, V. Tadigotla, M. Sigaroudinia, P. Gascard, T. Tlsty, J.F. Costello, I.M. Meyer, C.J. Eaves, W.W. Wasserman, S. Jones, D. Huntsman, M. Hirst, C. Caldas, M.A. Marra, S. Aparicio, The clonal and mutational evolution spectrum of primary triple-negative breast cancers, Nature 486 (7403) (2012) 395–399.
[10] G. Bianchini, J.M. Balko, I.A. Mayer, M.E. Sanders, L. Gianni, Triple-negative breast cancer: challenges and opportunities of a heterogeneous disease, Nat. Rev. Clin. Oncol. 13 (11) (2016) 674–690.
[11] K.A. Ryall, J. Kim, P.J. Klauck, J. Shin, M. Yoo, A. Ionkina, T.M. Pitts, J.J. Tentler, J.R. Diamond, S.G. Eckhardt, L.E. Heasley, J. Kang, A.C. Tan, An integrated bioinformatics analysis to dissect kinase dependency in triple negative breast cancer, BMC Genomics 16 (Suppl. 12) (2015) S2.
[12] J.S. Zawistowski, S.M. Bevill, D.R. Goulet, T.J. Stuhlmiller, A.S. Beltran, J.F. Olivares-Quintero, D. Singh, N. Sciaky, J.S. Parker, N.U. Rashid, X. Chen, J.S. Duncan, M.C. Whittle, S.P. Angus, S.H. Velarde, B.T. Golitz, X. He, C. Santos, D.B. Darr, K. Gallagher, L.M. Graves, C.M. Perou, L.A. Carey, H.S. Earp, G.L. Johnson, Enhancer remodeling during adaptive bypass to MEK inhibition is attenuated by pharmacologic targeting of the P-TEFb complex, Cancer Discov. 7 (3) (2017) 302–321.
[13] C. Saura, J. Bendell, G. Jerusalem, S. Su, Q. Ru, S. De Buck, D. Mills, S. Ruquet, A. Bosch, A. Urruticoechea, J.T. Beck, E. Di Tomaso, D.W. Sternberg, C. Massacesi, S. Hirawat, L. Dirix, J. Baselga, Phase Ib study of Buparlisib plus Trastuzumab in patients with HER2-positive advanced or metastatic breast cancer that has progressed on Trastuzumab-based therapy, Clin. Cancer Res. 20 (7) (2014) 1935–1945.
[14] F.M. Ferguson, N.S. Gray, Kinase inhibitors: the road ahead, Nat. Rev. Drug Discov. 17 (5) (2018) 353–377.
[15] J.S. Duncan, M.C. Whittle, K. Nakamura, A.N. Abell, A.A. Midland, J.S. Zawistowski, N.L. Johnson, D.A. Granger, N.V. Jordan, D.B. Darr, J. Usary, P.F. Kuan, D.M. Smalley, B. Major, X. He, K.A. Hoadley, B. Zhou, N.E. Sharpless, C.M. Perou, W.Y. Kim, S.M. Gomez, X. Chen, J. Jin, S.V. Frye, H.S. Earp, L.M. Graves, G.L. Johnson, Dynamic reprogramming of the kinome in response to targeted MEK inhibition in triple-negative breast cancer, Cell 149 (2) (2012) 307–321.
[16] A. Bahrami, M. Khazaei, S. Shahidsales, S.M. Hassanian, M. Hasanzadeh, M. Maftouh, G.A. Ferns, A. Avan, The therapeutic potential of PI3K/Akt/mTOR inhibitors in breast cancer: rational and progress, J. Cell. Biochem. 119 (1) (2018) 213–222.
[17] W. Wei, Y.S. Shin, M. Xue, T. Matsutani, K. Masui, H. Yang, S. Ikegami, Y. Gu, K. Herrmann, D. Johnson, X. Ding, K. Hwang, J. Kim, J. Zhou, Y. Su, X. Li, B. Bonetti, R. Chopra, C.D. James, W.K. Cavenee, T.F. Cloughesy, P.S. Mischel, J.R. Heath, B. Gini, Single-cell phosphoproteomics resolves adaptive signaling dynamics and informs targeted combination therapy in glioblastoma, Cancer Cell 29 (4) (2016) 563–573.
[18] C. Holohan, S. Van Schaeybroeck, D.B. Longley, P.G. Johnston, Cancer drug resistance: an evolving paradigm, Nat. Rev. Cancer 13 (10) (2013) 714–726.
[19] S. Chandarlapaty, Negative feedback and adaptive resistance to the targeted therapy of cancer, Cancer Discov. 2 (4) (2012) 311–319.
[20] G.O. Fruhwirth, L.P. Fernandes, G. Weitsman, G. Patel, M. Kelleher, K. Lawler, A. Brock, S.P. Poland, D.R. Matthews, G. Keri, P.R. Barber, B. Vojnovic, S.M. Ameer-Beg, A.C. Coolen, F. Fraternali, T. Ng, How Forster resonance energy transfer imaging improves the understanding of protein interaction networks in cancer biology, ChemPhysChem 12 (3) (2011) 442–461.
[21] Y. Fujita, N. Komatsu, M. Matsuda, K. Aoki, Fluorescence resonance energy transfer based quantitative analysis of feedforward and feedback loops in epidermal growth factor receptor signaling and the sensitivity to molecular targeting drugs, FEBS J. 281 (14) (2014) 3177–3192.
[22] K. Aoki, N. Komatsu, E. Hirata, Y. Kamioka, M. Matsuda, Stable expression of FRET biosensors: a new light in cancer research, Cancer Sci. 103 (4) (2012) 614–619.
[23] J.R. Conway, N.O. Carragher, P. Timpson, Developments in preclinical cancer imaging: innovating the discovery of therapeutics, Nat. Rev. Cancer 14 (5) (2014) 314–328.
[24] J. Zhang, M.D. Allen, FRET-based biosensors for protein kinases: illuminating the kinome, Mol. BioSyst. 3 (11) (2007) 759–765.
[25] J. Zhang, Y. Ma, S.S. Taylor, R.Y. Tsien, Genetically encoded reporters of protein kinase A activity reveal impact of substrate tethering, Proc. Natl. Acad. Sci. U.S.A. 98 (26) (2001) 14997–15002.
[26] K. Terai, M. Matsuda, Ras binding opens c-Raf to expose the docking site for mitogen-activated protein kinase kinase, EMBO Rep. 6 (3) (2005) 251–255.
[27] S. Regot, J.J. Hughey, B.T. Bajar, S. Carrasco, M.W. Covert, High-sensitivity measurements of multiple kinase activities in live single cells, Cell 157 (7) (2014) 1724–1734.
[28] N. Komatsu, K. Aoki, M. Yamada, H. Yukinaga, Y. Fujita, Y. Kamioka, M. Matsuda, Development of an optimized backbone of FRET biosensors for kinases and GTPases, Mol. Biol. Cell 22 (23) (2011) 4647–4656.
[29] H. Miura, M. Matsuda, K. Aoki, Development of a FRET biosensor with high specificity for Akt, Cell Struct. Funct. 39 (1) (2014) 9–20.
[30] Y. Zhang, M. Moerkens, S. Ramaiahgari, H. de Bont, L. Price, J. Meerman, B. van de Water, Elevated insulin-like growth factor 1 receptor signaling induces antiestrogen resistance through the MAPK/ERK and PI3K/Akt signaling routes, Breast Cancer Res. 13 (3) (2011) R52.
[31] R. Wang, G. He, M. Nelman-Gonzalez, C.L. Ashorn, G.E. Gallick, P.T. Stukenberg, M.W. Kirschner, J. Kuang, Regulation of Cdc25C by ERK-MAP kinases during the G2/M transition, Cell 128 (6) (2007) 1119–1132.
[32] C.D. Harvey, A.G. Ehrhardt, C. Cellurale, H. Zhong, R. Yasuda, R.J. Davis, K. Svoboda, A genetically encoded fluorescent sensor of ERK activity, Proc. Natl. Acad. Sci. U.S.A. 105 (49) (2008) 19264–19269.
[33] M.T. Kunkel, Q. Ni, R.Y. Tsien, J. Zhang, A.C. Newton, Spatio-temporal dynamics of protein kinase B/Akt signaling revealed by a genetically encoded fluorescent reporter, J. Biol. Chem. 280 (7) (2005) 5581–5587.
[34] A.J. Ridley, Membrane ruffling and signal transduction, BioEssays 16 (5) (1994) 321–327.
[35] S. Yoshida, R. Pacitto, C. Sesi, L. Kotula, J.A. Swanson, Dorsal ruffles enhance activation of Akt by growth factors, J. Cell Sci. 131 (22) (2018).
[36] J.L. Hoon, W.K. Wong, C.G. Koh, Functions and regulation of circular dorsal ruffles, Mol. Cell. Biol. 32 (21) (2012) 4246–4257.
[37] M.V. Repetto, M.J. Winters, A. Bush, W. Reiter, D.M. Hollenstein, G. Ammerer, P.M. Pryciak, A. Colman-Lerner, CDK and MAPK synergistically regulate signaling dynamics via a shared multi-site phosphorylation region on the scaffold protein Ste5, Mol. Cell 69 (6) (2018) 938–952 e6.
[38] S. Shukla, S. Gupta, Apigenin-induced cell cycle arrest is mediated by modulation of MAPK, PI3K-Akt, and loss of cyclin D1 associated retinoblastoma dephosphorylation in human prostate cancer cells, Cell Cycle 6 (9) (2007) 1102–1114.
[39] K. Ochodnicka-Mackovicova, M. Bahjat, T.A. Bloedjes, C. Maas, A.M. de Bruin, R.J. Bende, C.J. van Noesel, J.E. Guikema, NF-kappaB and AKT signaling prevent DNA damage in transformed pre-B cells by suppressing RAG1/2 expression and activity, Blood 126 (11) (2015) 1324–1335.
[40] M.M. Lahair, C.J. Howe, O. Rodriguez-Mora, J.A. McCubrey, R.A. Franklin, Molecular pathways leading to oxidative stress-induced phosphorylation of Akt, Antioxid. Redox Signal. 8 (9–10) (2006) 1749–1756.
[41] M.C. Mendoza, E.E. Er, J. Blenis, The Ras-ERK and PI3K-mTOR pathways: cross-talk and compensation, Trends Biochem. Sci. 36 (6) (2011) 320–328.
[42] R.L.B. Costa, H.S. Han, W.J. Gradishar, Targeting the PI3K/AKT/mTOR pathway in triple-negative breast cancer: a review, Breast Cancer Res. Treat. 169 (3) (2018) 397–406.
[43] S. Gross, R. Rahal, N. Stransky, C. Lengauer, K.P. Hoeflich, Targeting cancer with kinase inhibitors, J. Clin. Invest. 125 (5) (2015) 1780–1789.
[44] H. Xu, P. Eirew, S.C. Mullaly, S. Aparicio, The omics of triple-negative breast cancers, Clin. Chem. 60 (1) (2014) 122–133.
[45] F. Sanchez-Vega, M. Mina, J. Armenia, W.K. Chatila, A. Luna, K.C. La, S. Dimitriadoy, D.L. Liu, H.S. Kantheti, S. Saghafinia, D. Chakravarty, F. Daian, Q.S. Gao, M.H. Bailey, W.W. Liang, S.M. Foltz, I. Shmulevich, L. Ding, Z. Heins, A. Ochoa, B. Gross, J.J. Gao, H.X. Zhang, R. Kundra, C. Kandoth, I. Bahceci, L. Dervishi, U. Dogrusoz, W.D. Zhou, H. Shen, P.W. Laird, G.P. Way, C.S. Greene, H. Liang, Y.H. Xiao, C. Wang, A. Iavarone, A.H. Berger, T.G. Bivona, A.J. Lazar, G.D. Hammer, T. Giordano, L.N. Kwong, G. McArthur, C.F. Huang, A.D. Tward, M.J. Frederick, F. McCormick, M. Meyerson, E.M. Van Allen, A.D. Cherniack, G. Ciriello, C. Sander, N. Schultz, C.G.A.R. Network, Oncogenic signaling pathways in the cancer genome atlas, Cell 173 (2) (2018) 321-+.
[46] E. Andreopoulou, C.M. Kelly, H.M. McDaid, Therapeutic advances and new directions for triple-negative breast cancer, Breast Care (Basel) 12 (1) (2017) 21–28.
[47] M.D. Wallace, A.D. Pfefferle, L. Shen, A.J. McNairn, E.G. Cerami, B.L. Fallon, V.D. Rinaldi, T.L. Southard, C.M. Perou, J.C. Schimenti, Comparative oncogenomics implicates the neurofibromin 1 gene (NF1) as a breast cancer driver, Genetics 192 (2) (2012) 385–396.
[48] J.M. Balko, R.S. Cook, D.B. Vaught, M.G. Kuba, T.W. Miller, N.E. Bhola, M.E. Sanders, N.M. Granja-Ingram, J.J. Smith, I.M. Meszoely, J. Salter, M. Dowsett, K. Stemke-Hale, A.M. Gonzalez-Angulo, G.B. Mills, J.A. Pinto, H.L. Gomez, C.L. Arteaga, Profiling of residual breast cancers after neoadjuvant chemotherapy identifies DUSP4 deficiency as a mechanism of drug resistance, Nat. Med. 18 (7) (2012) 1052–1059.
[49] C. Gewinner, Z.C. Wang, A. Richardson, J. Teruya-Feldstein, D. Etemadmoghadam, D. Bowtell, J. Barretina, W.M. Lin, L. Rameh, L. Salmena, P.P. Pandolfi, L.C. Cantley, Evidence that inositol polyphosphate 4-phosphatase type II is a tumor suppressor that inhibits PI3K signaling, Cancer Cell 16 (2) (2009) 115–125.
[50] Y.H. Li, P.P. Wang, X.X. Li, C.Y. Yu, H. Yang, J. Zhou, W.W. Xue, J. Tan, F. Zhu, The human kinome targeted by FDA approved multi-target drugs and combination products: a comparative study from the drug-target interaction network perspective, PLoS One 11 (11) (2016).
[51] V. Kothari, I. Wei, S. Shankar, S. Kalyana-Sundaram, L. Wang, L.W. Ma, P. Vats, C.S. Grasso, D.R. Robinson, Y.M. Wu, X. Cao, D.M. Simeone, A.M. Chinnaiyan, C. Kumar-Sinha, Outlier kinase expression by RNA sequencing as targets for precision therapy, Cancer Discov. 3 (3) (2013) 280–293.
[52] M. Dermit, A. Dokal, P.R. Cutillas, Approaches to identify kinase dependencies in cancer signalling networks, FEBS Lett. 591 (17) (2017) 2577–2592.
[53] M. Sun, G. Wang, J.E. Paciga, R.I. Feldman, Z.Q. Yuan, X.L. Ma, S.A. Shelley, R. Jove, P.N. Tsichlis, S.V. Nicosia, J.Q. Cheng, AKT1/PKBalpha kinase is frequently elevated in human cancers and its constitutive activation is required for oncogenic transformation in NIH3T3 cells, Am. J. Pathol. 159 (2) (2001) 431–437.
[54] S. Kilpinen, K. Ojala, O. Kallioniemi, Analysis of kinase gene expression patterns across 5681 human tissue samples reveals functional genomic taxonomy of the kinome, PLoS One 5 (12) (2010) e15068.